Efficient Simulation of Three-Pulse Photon-Echo Signals with Application to the Determination of Electronic Coupling in a Bacterial Photosynthetic Reaction Center†

Yuan-Chung Cheng, Hohjai Lee, and Graham R. Fleming*

Department of Chemistry and QB3 Institute, University of California Berkeley, and Physical Bioscience Division, Lawrence Berkeley National Laboratory, Berkeley, California 94720

Received: May 8, 2007; In Final Form: June 25, 2007

A time-nonlocal quantum master equation coupled with a perturbative scheme to evaluate the third-order polarization in the phase-matching direction $\mathbf{k}_s = -\mathbf{k}_1 + \mathbf{k}_2 + \mathbf{k}_3$ is used to efficiently simulate three-pulse photon-echo signals. The present method is capable of describing photon-echo peak shifts including pulse overlap and bath memory effects. In addition, the method treats the non-Markovian evolution of the density matrix and the third-order polarization in a consistent manner, thus is expected to be useful in systems with rapid and complex dynamics. We apply the theoretical method to describe one- and two-color three-pulse photon-echo peak shift experiments performed on a bacterial photosynthetic reaction center and demonstrate that, by properly incorporating the pulse overlap effects, the method can be used to describe simultaneously all peak shift experiments and determine the electronic coupling between the localized Q_y excitations on the bacteriopheophytin (BPhy) and accessory bateriochlorophyll (BChl) in the reaction center. A value of $J = 250\ \mathrm{cm}^{-1}$ is found for the coupling between BPhy and BChl.

1. Introduction

Recent advances in ultrafast spectroscopy have enabled experimental study of dynamics in strongly coupled multichromophoric systems.[1−3] In particular, the three-pulse photon-echo (3PPE) technique had been used to study energy transfer dynamics in photosynthetic complexes[4−8] and solvation dynamics in liquids,[9−11] glasses,[5,12,13] and proteins.[4,14,15] Recently, the two-color three-pulse photon-echo peak shift (2C3PEPS) technique has proven to be an useful probe for the electronic coupling and energy transfer dynamics between excitations in coupled multichromophoric systems.[8,16] Because the 2C3PEPS is sensitive to correlated spectral motion between two regions of optical excitation, it is a direct probe of electronic coupling between chromophores. In the limit of slow population transfer, the analytical formula proposed by Yang and Fleming and later extended by Mancal and Fleming can be used to estimate electronic coupling between chromophores.[17−19] However, for systems with excitation energy transfer in the time scale comparable to the bath relaxation time scale, the analytical expression is not valid and it is necessary to simulate the 2C3PEPS data based on a theoretical model to estimate the electronic couplings.[20] Therefore, interpretation of these experiments depends critically on our ability to describe coupled multichromophoric systems using reasonable models including exciton−exciton interaction, exciton−phonon coupling, and static disorder.

In the standard response function formalism of nonlinear spectroscopy, the 3PPE experiments are described by the third-order polarization, which can be calculated from impulsive response functions of the material system.[1] The response function formalism has been successfully applied to describe various third-order nonlinear techniques. However, when ultrafast excitation energy transfer dynamics is involved in the system, additional time propagators of the system have to be calculated by invoking additional approximations[21,22] or obtained using other dynamical theories and inserted into the response functions.[7,17,19,23] In addition, when the dynamical time scale of the system is comparable to the pulse duration, the pulse overlap effect can be significant and triple convoluted time integrals over the pulse profiles and the incorporation of additional response function terms are required to describe the experiments. These additional requirements can substantially reduce efficiency of the response function simulations. Therefore, a theoretical description of third-order nonlinear spectroscopy in which the system dynamics is treated efficiently and consistently with the response of the system is needed.

Another theoretical approach to the calculation of nonlinear spectroscopic signals is via a nonperturbative description of the nonlinear polarization.[24−26] By including the field-material interaction explicitly and propagating the reduced density matrix of the system exactly, the third-order polarization that describes various third-order nonlinear techniques can be calculated nonperturbatively.[24,25,27−29] However, the nonperturbative approach is computationally expensive because the calculation results in the total polarization. To extract the signal corresponding to a specific experiment, one needs to compute the total polarization at different phase angles and determine the contribution to a specific phase-matching direction by solving a linear matrix equation at each time step, and this extraction procedure is quite inefficient. As a result, it is computationally infeasible to apply the nonpertubative approach to general multichromophoric systems.

Recently, an efficient method to calculate third-order polarization via a perturbative procedure was proposed by Gelin et al.[30] This method greatly reduces the effort needed to extract

† Part of the "Sheng Hsien Lin Festschrift".

* To whom correspondence should be addressed. E-mail: GRFleming@lbl.gov.

10.1021/jp0735177 CCC: $37.00
Published on Web 08/14/2007

the third-order polarization that contributes to the 3PPE signals and can be applied to systems with higher dimensions. In this paper, we extend this perturbative method to describe multichromophoric systems and static disorder. More specifically, we present a more complete description of the third-order 3PPE polarization by including two-excitation states in the theory and using a time-nonlocal quantum master equation to properly describe the bath memory effect that is critical for three-pulse photon-echo peak shift (3PEPS). To demonstrate the potential of the generalized method, we apply it to simulate 3PEPS experiments performed on a bacterial photosynthetic reaction center (RC) and determine the electronic coupling between the localized Q_y excitations on the bacteriopheophytin and accessory bateriochlorophyll in the RC.

2. Theoretical Methods

2.1. Exciton Hamiltonian. We consider the following total system-plus-bath Hamiltonian

$$H_T = H_S + H_{int} + H_B + H_{SB} \tag{1}$$

where H_S is the Hamiltonian of the electronic system, H_{int} describes the interaction of the system to the laser fields, H_B is the bath Hamiltonian, and H_{SB} describes the system−bath interaction. For the system part, we use a Frenkel-exciton model to describe a multichromophoric system made of N two-level chromophores[31]

$$H_S = \epsilon_g|0\rangle\langle 0| + \sum_{n=1}^{N}\epsilon_n a_n^\dagger a_n + \sum_{n,m}^{n\neq m} J_{nm} a_n^\dagger a_m \tag{2}$$

where $|0\rangle$ denotes the electronic ground state, a_n ($a_n^\dagger$) is the annihilation (creation) operator that destroys (creates) an excitation at site n, ϵ_g is the energy of the ground state, ϵ_n is the site energy at the nth chromophore, and J_{nm} is the electronic coupling between the nth and mth chromophores. a_n and $a_n^\dagger$ describe electronic transitions between the molecular ground and excited states. They satisfy the Pauli commutation relations

$$[a_n, a_m^\dagger] = \delta n_m(1 - 2a_n^\dagger a_n), \qquad [a_n, a_m] = 0 \tag{3}$$

The H_{int} term denotes the system−field interaction in the electric point dipole approximation, $H_{int}(t) = -\hat{\mu}\mathbf{E}(t)$, where the dipole operator in the second-quantized form is defined as

$$\hat{\mu} = \sum_{n=1}^{N}\vec{\mu}_n(a_n + a_n^\dagger) \tag{4}$$

Explicit inclusion of the system−field interaction allows us to treat the driven dynamics of the system exactly and use the result to compute the third-order polarization. Finally, we assume a harmonic bath of independent harmonic oscillators for H_B, and the electronic system is coupled linearly to the bath through a number of collective bath coordinates q_m:

$$H_{SB} = -\sum_i S_i q_i \tag{5}$$

where S_i is a general system operator in the one-excitation subspace, and q_i denotes a collective bath coordinate that is coupled to the system through the S_i operator. For example, $S = a_n^\dagger a_n$ represents the energetic diagonal coupling of the localized excitation on the nth chromophore to the bath. Without loss of generality, we also assume that baths coupled to different system operators are independent, i.e., $C_{ij}(t) = \langle q_i(t)q_j(0)\rangle$ is zero when $i \neq j$. Note that we do not limit S to be a local operator, therefore, nonlocal bath effects can be taken into account by considering a nonlocal S.

To describe the third-order polarization, it is necessary to consider up to two-exciton states.[21,22,31] To this end, we consider the electronic system in the Hilbert space span by the subspace of the ground state ($\mathscr{H}_g$), the one-excitation states ($\mathscr{H}_e^1$), and the two-excitation states ($\mathscr{H}_e^2$). In the site representation, $\mathscr{H}_e^1$ for N two-level chromophores is spanned by the basis consist of N one-excitation states, $|n\rangle = a_n^\dagger|0\rangle$, $n = 1...N$, and $\mathscr{H}_e^2$ is spanned by $N(N-1)/2$ two-excitation states $|nm\rangle$ defined as $|nm\rangle = a_n^\dagger a_m^\dagger|0\rangle$ for all $n \neq m$ and $m > n$. Using the exciton commutation rule in eq 3, any operators in the $\mathscr{H}_e^1$ subspace, $O = \sum_{nm}O_{nm}a_n^\dagger a_m$, can be expanded to $\mathscr{H}_e^2$ using

$$\langle nm|O|n'm'\rangle = \delta_{nm'}O_{mm'} + \delta_{mn'}O_{nm'} + \delta_{nm'}O_{mn'} + \delta_{mm'}O_{nn'} \tag{6}$$

For example, the exciton Hamiltonian in eq 2 can be represented in the full $\mathscr{H}_g \otimes \mathscr{H}_e^1 \otimes \mathscr{H}_e^2$ Hilbert space, and the diagonalization of the full matrix will result in manifolds of a ground state, N one-exciton states, and $N(N-1)/2$ two-exciton states.

The dipole operator that connects the $\mathscr{H}_g$ and $\mathscr{H}_e^1$ subspaces can be extended to the $\mathscr{H}_e^1 \otimes \mathscr{H}_e^2$ subspace using

$$\begin{aligned}\langle n|\hat{\mu}|n'm'\rangle &= \vec{\mu}_{n'}\delta_{nm'} + \vec{\mu}_{m'}\delta_{nn'}\\ \langle n|\hat{\mu}|m\rangle &= 0\\ \langle nm|\hat{\mu}|n'm'\rangle &= 0\end{aligned} \tag{7}$$

Equations 6 and 7 enable us to expand all system operators in the ground and one-excitation subspace to the two-excitation manifold. This allows us to treat excitonic dynamics in the one- and two-excitation subspace in a consistent manner. Note that this is possible because, in the exciton Hamiltonian (eq 2), all nonresonant interactions between excitations are neglected (Heitler−London approximation), and we assume that there is no coupling between one- and two-excitation manifolds (no configuration interaction). These approximations are reasonable for excitations in photosynthetic pigment−protein complexes.[31,32]

2.2. Perturbative Evaluation of the Third-Order Polarization. We consider a four-wave mixing experiment described in Figure 1 in which three laser pulses interact with the sample to create a polarization. The induced third-order polarization $P^{(3)}(t)$ then radiates into the phase-matching directions $\pm\mathbf{k_1}\pm\mathbf{k_2}\pm\mathbf{k_3}$. Experimentally, two time delays, the coherence time τ and the population time T, can be varied to study the dynamics of the optical excitations induced by the laser fields interacting with the system. In this paper, we will focus on the 3PPE experiments in which the signal in the phase-matching direction $\mathbf{k_s} = -\mathbf{k_1} + \mathbf{k_2} + \mathbf{k_3}$ is measured. In particular, we will present a theoretical method that can be used to evaluate the 3PEPS for a general multichromophoric system. In a 3PEPS experiment, the integrated intensity of the echo signals at fixed T is measured while varying τ. The peak maximum shift from $\tau = 0$ (peak shift) is recorded, and its value as a function of T constitutes the 3PEPS spectrum. The 3PEPS usually shows decay as a function of T, and the decay is directly related to the time-correlation function of the fluctuations of the optical transition frequency modulated by the bath modes coupled to the excitation.[1,9,10] Therefore, the 3PEPS measurement provides information on the electron−phonon couplings in the system.

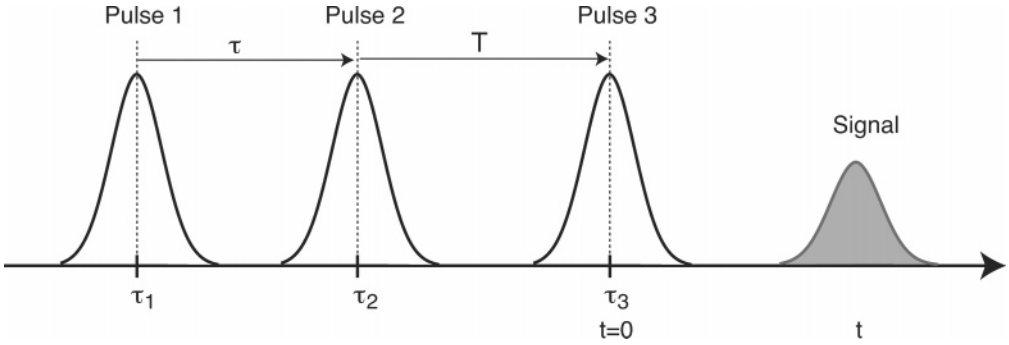

Figure 1. Three-pulse photon-echo experiment and definition of time variables. Three laser pulses centered at τ_1, τ_2, and τ_3 are incident on the sample to generate a signal field. The coherence time τ is defined as $\tau = \tau_2 - \tau_1$, and the population time $T = \tau_3 - \tau_2$. The pulse sequence depicted here gives positive τ and T. The time zero $t = 0$ is set at the center of the third pulse.

Theoretically, the integrated photon-echo signal is described by the third-order polarization $P^{(3)}_{3PPE}(t)$,

$$S(\tau,T) \sim \int_0^\infty dt |P^{(3)}_{3PPE}(t)|^2 \quad (8)$$

Therefore, a theoretical description of 3PPE experiments requires the determination of $P^{(3)}_{3PPE}(t)$. In the standard perturbative approach to nonlinear spectroscopy, the third-order polarization is represented by response functions.[1] Here we consider another approach that incorporates the system−field interactions explicitly in the time evolution of the density matrix of the system. In general, the time evolution of the reduced density matrix of a quantum system $\rho(t)$ can be described by a quantum master equation[33−35]

$$\dot{\rho}(t) = -i[H_S + H_{int}(t),\rho(t)] - \mathscr{R}[\rho(t)] \quad (9)$$

where $H_S + H_{int}(t)$ is the time-dependent Hamiltonian defined in eqs 1−4 that governs the coherent evolution of the system, and $\mathscr{R}[\cdot]$ represents the dissipative dynamics of the system induced by the system−bath interactions. The time-dependent total polarization induced by the laser fields is the expectation value of the dipole operator

$$P(t) = \langle \hat{\mu}\rho(t)\rangle \quad (10)$$

where the bracket $\langle\cdots\rangle$ means taking the expectation value of the operator and average over static disorder. When the system−field interaction $H_{int}(t)$ is explicitly included in the time propagation of the density matrix, the reduced density matrix $\rho(t)$ contains all the information on the time-dependent optical response of the material system. However, the total polarization obtained using eq 10 contains fields that radiate into all directions and thus does not describe a real experiment in which only signals in a specific phase-matching direction are measured. In the response function formalism, the signal in the phase-matching direction is well defined because each response function corresponds to a Liouville space pathway and its radiation direction is fixed in the rotating wave approximation (RWA). However, in a density matrix based method, the direction (phase) is not obvious and extra analysis is required to extract the signals in the phase-matching direction of the experiment. The nonperturbative method allows such analysis by varying phase angles associated with the fields and then solving a set of complicated matrix equations (or performing discrete Fourier transform) to extract the experimental signal. However, because the procedure is computationally intensive, the nonperturbative approach is limited to small systems.[24,26] Here we instead adopt the efficient perturbative method proposed by Gelin et al. to extract the 3PPE signal.[30]

Consider a four-wave mixing experiment in which the three laser pulses are described by the time-dependent electric field

$$\mathbf{E}(t) = \sum_{a=1}^{3} [E_a(t-\tau_a)\exp\{-i(\omega_a t - k_a r)\} + cc] \quad (11)$$

where $E_a(t-\tau_a)$ is the laser pulse profile, ω_a is the carrier frequency, and k_a is the momentum. In this work, we will adopt a Gaussian pulse profile $E_a(t) \sim \exp(-4\ln 2(t-\tau_a)^2/\tau_p^2)$, where τ_p is the pulse duration defined by the full width at half-maximum (fwhm) of the pulse profile. Gelin et al. showed that the third-order polarization in the 3PPE phase-matching direction $\mathbf{k_s} = -\mathbf{k_1} + \mathbf{k_2} + \mathbf{k_3}$ can be calculated by following the time evolution of seven auxiliary density matrices.[30] Following Gelin et al., we define the operator

$$V_a(t) = E_a(t-\tau_a)\exp(i\omega_a t)\hat{\mu} \quad (12)$$

and seven auxiliary density matrices through the following equations of motion

$$\begin{aligned}
\partial_t\rho_1(t) &= -i[H_S - V_1(t) - V_2^\dagger(t) - V_3^\dagger(t),\rho_1(t)] - \mathscr{R}[\rho_1(t)]\\
\partial_t\rho_2(t) &= -i[H_S - V_1(t) - V_2^\dagger(t),\rho_2(t)] - \mathscr{R}[\rho_2(t)]\\
\partial_t\rho_3(t) &= -i[H_S - V_1(t) - V_3^\dagger(t),\rho_3(t)] - \mathscr{R}[\rho_3(t)]\\
\partial_t\rho_4(t) &= -i[H_S - V_1(t),\rho_4(t)] - \mathscr{R}[\rho_4(t)]\\
\partial_t\rho_5(t) &= -i[H_S - V_2^\dagger(t) - V_3^\dagger,\rho_5(t)] - \mathscr{R}[\rho_5(t)]\\
\partial_t\rho_6(t) &= -i[H_S - V_2^\dagger(t),\rho_6(t)] - \mathscr{R}[\rho_6(t)]\\
\partial_t\rho_7(t) &= -i[H_S - V_3^\dagger(t),\rho_7(t)] - \mathscr{R}[\rho_7(t)]
\end{aligned} \quad (13)$$

Note that we do not invoke the RWA here. Numerically, it is more convenient if the RWA is invoked in the propagation of eq 13 because the fast oscillating terms are neglected.[30] Instead, we choose to perform the propagation in the interaction picture of H_S to avoid treating fast oscillating dynamics explicitly. Equations 12−13 can be used to propagate the seven auxiliary density matrices, and the 3PPE polarization can be calculated using

$$P^{(3)}_{3PPE}(t) = \langle\hat{\mu}(\rho_1(t) - \rho_2(t) - \rho_3(t) + \rho_4(t) - \rho_5(t) + \rho_6(t) + \rho_7(t))\rangle \quad (14)$$

where $\hat{\mu}$ is the dipole operator defined in eq 4. Equation 14 is a system of seven independent linear differential equations. Although propagating seven density matrices seems to be a

significant overhead in the calculation, the propagation of these auxiliary density matrices can be performed independently and made into parallelized program codes, which means that the time propagation required to calculate $P^{(3)}_{3PPE}(t)$ can be implemented efficiently in modern computer systems. Thus, eqs 13−14 provide an efficient prescription for the calculation of the 3PPE signals. Note that eq 14 is obtained by using a perturbative approach, therefore although the system−field interactions are treated exactly, the applicability of eq 14 depends on the optical field being weak. This is in contrast to the nonperturbative approach that is valid for all field strengths. As a result, like the response function approach, the current method is limited to experiments in the weak-field limit. In this formalism, both system−field interactions and chromophore excitonic couplings are treated exactly, while the bath-induced dissipative dynamics have to be treated perturbatively. In the next section, we will describe the dissipative dynamics.

2.3. Non-Markovian Evolution in the Presence of Laser Fields. The dissipative dynamics of the system can be treated by considering a system−bath model in which the bath degrees of freedom are traced out at the end of the calculation to obtain the reduced density matrix of the system. In this section, we consider the effect of the system−bath interaction defined in eq 5. Without loss of generality, in this section, we will consider only one system−bath coupling term $H_{SB} = -S\cdot q$ and drop the i index in eq 5. It is trivial to extend the results to include multiple system−bath coupling terms.

We emphasize that a formulation of the quantum master equation that includes non-Markovian dynamics and bath memory effects is necessary for the description of 3PEPS experiments because non-Markovian bath memory effects are essential for a system to exhibit a peak shift. This is not a problem in the standard response function approach because the response functions corresponding to various Liouville pathways automatically track the history of the system and the non-Markovian effect of the bath is included in the cumulant expansion method generally used to treat the diagonal electron−phonon couplings in the one-exciton basis. Therefore, although it is usually necessary to ignore the memory effects in the dynamics induced by the off-diagonal electron−phonon couplings in the response function approach (for example, memory effects in energy transfer), calculations based on response functions still describe peak shifts. However, for the nonperturbative approach or the perturbative approach described in Section 2.2, the bath memory effects must be included in the quantum master equation that is used to propagate the driven dynamics of the system. Mancal et al. pointed out that, if Redfield theory is used to propagate the density matrix in a nonperturbative approach to evaluate the third-order polarization, the result does not give a peak shift[28] because the bath memory effects are neglected in the Redfield theory.[34,36] The Redfield formalism was used in the nonperturbative approach to propagate the reduced density matrix and calculate the 3PEPS and electronic 2D spectra for excitonic systems,[27−29] however, the propagation given by the Redfield theory does not describe peak shifts properly unless the system is dominated by inhomogeneous broadenings. To describe peak shifts, we need to use a theory for the dissipative part of the dynamics that includes the bath memory effects. To this end, we use the time-nonlocal formalism proposed by Meier and Tannor.[36,37]

We start with the time-nonlocal (TNL, also called time-convolution approach or chronological time-ordering prescription) quantum master equation derived by using the projection operator technique and neglecting terms up to the second-order in the system−bath interactions:[34]

$$\partial_t \rho(t) = -i\mathscr{L}_S^{\text{eff}}\rho(t) + \int_0^t \mathrm{d}\tau \mathscr{K}(t,\tau)\rho(\tau) \tag{15}$$

where

$$\mathscr{L}_S^{\text{eff}} = [H_S + H_{\text{int}}(t) + H_{\text{ren}},\cdot]$$

$$\mathscr{K}(t,\tau) = \mathscr{L}_- \exp_+{}^{-i\int_\tau^t \mathrm{d}t_1 \mathscr{L}_S(t_1)} [a(t-\tau)\mathscr{L}_- + b(t-\tau)\mathscr{L}_+]$$

$$\mathscr{L}_S = [H_S + H_{\text{int}}(t),\cdot]$$

$$\mathscr{L}_- = -i[S,\cdot],\ \mathscr{L}_+ = [S,\cdot]_+$$

$$H_{\text{ren}} = \frac{1}{2}V_{\text{ren}}S^2 \tag{16}$$

and $a(t)$ and $b(t)$ are the real part and the negative imaginary part of the bath correlation function, $C(t) = \langle q(t)q(0)\rangle = a(t) - ib(t)$, respectively. H_{ren} is the renormalization Hamiltonian that is required in order to avoid artificial shifts in the system energy due to the coupling to the bath.[35] The renormalization potential V_{ren} can be calculated in terms of the spectral density of the bath, $V_{\text{ren}} = 2/\pi\int_0^\infty \mathrm{d}\omega J(\omega)/\omega$. In addition, we have assumed that the total system is initially a product state of the ground state ($\rho(0) = |g\rangle\langle g|$) and the equilibrium bath, so that the inhomogeneous term in the TNL quantum master equation vanishes.

The integral in eq 15 refers to the reduced density matrix of the system at all times, which makes the direct propagation of eq 15 very difficult. Following Meier and Tannor, we recast the quantum master equation into a more convenient form by adopting an artificial bath model in which the bath spectral density is in the following form:

$$J(\omega) = \sum_{k=1}^{n} \frac{4\lambda_k \Gamma_k{}^3 \omega}{[(\omega+\Omega_k)^2 + \Gamma_k{}^2][\omega - \Omega_k)^2 + \Gamma_k{}^2]} \tag{17}$$

where the bath spectral density is decomposed into n terms, and λ_k, Ω_k, and Γ_k are real parameters describe the kth bath mode. The decomposition can be used to simulate arbitrary bath spectral densities. For example, the Ohmic spectral density with exponential cutoff can be represented by three terms ($n = 3$).[37] This artificial bath model describes modes that range from overdamped oscillators (when $\Gamma_k \gg \Omega_k$) to coherent oscillators (when $\Omega_k \gg \Gamma_k$). As a result, the bath model is capable of describing a wide range of bath-induced dynamics on the system. This is even more useful when one attempts to describe experimental data because the ansatz offers a flexible basis that can extract a wealth of dynamical information from experimental data.

The bath time correlation function which describes the memory kernel in eq 16 can be represented in terms of $J(\omega)$:

$$\begin{aligned} C(t) &= \langle q(t)q(0)\rangle \\ &= \frac{1}{\pi}\int_0^\infty J(\omega)\cos(\omega t)\coth(\beta\omega/2)\,\mathrm{d}\omega - \\ &\qquad \frac{i}{\pi}\int_0^\infty J(\omega)\sin(\omega t)\,\mathrm{d}\omega \\ &\equiv a(t) - ib(t) \end{aligned} \tag{18}$$

The real part and negative imaginary part of the correlation for the artificial bath model in eq 17 can then be obtained analytically

$$a(t) = \sum_{k=1}^{n} \frac{\lambda_k \Gamma_k^2}{2\Omega_k} \{\coth(\beta\Omega_k^-/2)\, e^{-i\Omega_k^- t} + \coth(\beta\Omega_k^+/2)\, e^{i\Omega_k^+ t}\} + \frac{2i}{\beta} \sum_{k=1}^{n_m} J(i\nu_k)\, e^{-\nu_k t}$$

$$b(t) = -i \sum_{k=1}^{n} \frac{\lambda_k \Gamma_k^2}{2\Omega_k} \{e^{-i\Omega_k^- t} + e^{i\Omega_k^+ t}\} \tag{19}$$

where we have defined $\Omega_k^+ = \Omega_k + i\Gamma_k$, $\Omega_k^- = \Omega_k - i\Gamma_k$, and β is the inverse temperature. The last part in $a(t)$ is the Matsubara terms with Matsubara frequency $\nu_k = 2\pi k/\beta$. The sum over Matsubara terms is an infinite one, but in practice we can truncate the sum at a finite number of n_m terms, especially at higher temperatures. In eq 19, $a(t)$ and $b(t)$ can be expressed by $n_r = 2n + n_m$ and $n_i = 2n$ exponential terms, respectively. Therefore, we can write $a(t)$ and $b(t)$ as sum of exponentials $a(t) = \sum_{k=1}^{n_r} \alpha_k^r\, e^{\gamma_k^r t}$, and $b(t) = \sum_{k=1}^{n_i} \alpha_k^i\, e^{\gamma_k^i t}$, where α_k^r, α_k^i, γ_k^r, and γ_k^i are complex coefficients defined by eq 19. This exponential form of the correlation function allows us to recast the time-nonlocal quantum master equation into a set of coupled time-local, first-order differential equations[36,37]

$$\begin{aligned}
\rho(t) &= -i\mathscr{L}_S^{\text{eff}}\rho(t) + \mathscr{L}_-\{\sum_{k=1}^{n_r}\alpha_k^r \rho_k^r(t) + \sum_{k=1}^{n_i}\alpha_k^i \rho_k^i(t)\} \\
\rho_k^r(t) &= \mathscr{L}_-\rho(t) + (\gamma_k^r - i\mathscr{L}_S)\rho_k^r(t) \\
\rho_k^i(t) &= \mathscr{L}_+\rho(t) + (\gamma_k^i - i\mathscr{L}_S)\rho_k^i(t)
\end{aligned} \tag{20}$$

Note that, in order to propagate the TNL dynamics, additional auxiliary matrices ρ_k^r and ρ_k^i are introduced. Propagating these additional matrices entails a significant overhead on the efficiency of the calculation, but it is necessary in order to include bath memory effects. Equation 20 is the final form of the TNL quantum master equation that we use to propagate $\rho_1(t) - \rho_7(t)$ in eq 13 and then calculate $P_{3\text{PPE}}^{(3)}(t)$ according to eq 14. In addition, to properly describe the third-order polarization, it is necessary to include contributions from the two-excitation states. Therefore, all operators in eq 20 have to be considered in the full $\mathscr{H}_g \otimes \mathscr{H}_e^1 \otimes \mathscr{H}_e^2$ Hilbert according to eqs 6 and 7. In our simulation, we numerically propagate the TNL dynamics using an iterated Crank−Nicholson scheme.[38] To calculate the 3PEPS as a function of the population time T, we compute the integrated signal $S(\tau,T)$ (eq 8) on a two-dimensional grid of coherence time (τ) and population time (T) points and then use a numerical cubic spline interpolation algorithm to determine the peak shift from $\tau = 0$.

This formalism seems to be limited to weak exciton−phonon couplings because the TNL quantum master equation is based on the assumption that the system−bath interactions are weak and that neglect of higher-order terms in the memory kernels is valid. This weak-coupling condition may not be a serious limitation, however, because in many physical scenarios, the system is strongly coupled to only a few bath modes. Therefore, the system−bath boundary can be redefined to include strongly coupled modes into the system, and the weak coupling approximation can still be employed.

2.4. Static Disorder. So far, we have focused on the calculation of third-order polarization for a single system with well-defined system Hamiltonian. To include the effects of static disorder, an average of the third-order polarization over a statistical distribution of systems is required. Conventionally, Monte Carlo (MC) sampling is used to average the signal over a statistic distribution of transition frequencies.[39] However, an MC average usually requires repeating the calculation for thousands of realizations of the system Hamiltonian in order to achieve reasonable convergence. The MC average procedure is inefficient and frequently the bottleneck of a simulation of nonlinear spectroscopic signals. Thus, a more efficient means to perform the average over static disorder would significantly improve our ability to simulate and describe experimental results.

We consider diagonal energetic disorder on each site described by a random variable $\delta\epsilon_n$, which is defined by a Gaussian distribution with zero mean ($\langle\delta\epsilon_n\rangle = 0$) and standard deviation σ_n. The average over the distribution of static energetic disorder can be represented by Gaussian integral over all disorder random variables:

$$\langle P(\tau, T, t)\rangle_{\text{static}} = \int_{-\infty}^{\infty} d\Gamma(\delta\epsilon) \prod_n e^{-\delta\epsilon_n^2/2\sigma_n^2} P(\Gamma(\delta\epsilon); \tau,T,t) \tag{21}$$

where $\Gamma(\delta\epsilon)$ is a vector representing the random variables $\{\delta\epsilon_n\}$. If the integrand $P(\Gamma(\delta\epsilon); \tau,T,t)$ is smooth within the Gaussian profile, which is satisfied when the static disorder σ_n is small compared to the characteristic frequency of the polarization (usually the differences between transition frequencies of excitations), the Gaussian weighted integral can be evaluated most efficiently using the Gauss−Hermite quadrature method.[40] Therefore, a more efficient way than MC sampling is to evaluate $P(\Gamma(\delta\epsilon); \tau,T,t)$ using the Gauss−Hermite rule for each random variable $\delta\epsilon_n$. For high-dimensional systems with many random variables, high-dimensional quadrature rules exist that can be used to estimate the integral in eq 21 efficiently.[40,41] In addition, the numerical method can be generalized to treat more general forms of static disorder such as correlated energetic disorder or off-diagonal static disorder without any additional computational efforts.

3. 3PEPS of a Model Two-Level System

To demonstrate our new approach for the calculation of 3PEPS signal, we consider a simple two-level system (ground state and excited state) and study the effects of pulse overlap and static disorder. In the calculations, we assume a model two-level system coupled to a single overdamped bath mode with $\lambda_0 = 150\ \text{cm}^{-1}$, $\Omega_0 = 50\ \text{cm}^{-1}$, $\Gamma_0 = 80\ \text{cm}^{-1}$, and that the laser pulse frequency is on resonance with the optical $|g\rangle \rightarrow |e\rangle$ transition. In addition, a Gaussian static disorder with standard deviation $\sigma_s = 100\ \text{cm}^{-1}$ is also included.

We first compare the Gauss−Hermite quadrature method for the average over Gaussian static disorder to the standard MC sampling method. In Figure 2, we show the results calculated using a 11-point Gauss−Hermite rule and an average over 5000 realizations using MC sampling over a Gaussian distribution. The peak shift decays to a finite value at large population time, which is a signature for systems with static disorder. With $\sigma_s = 100\ \text{cm}^{-1}$, the Gaussian sampling is not converged when 5000 random points are used; in contrast, the Gauss−Hermite rule gives a satisfactory result with 11 points.

In Figure 3, we show the 3PEPS for the model system calculated using different pulse widths. The result calculated

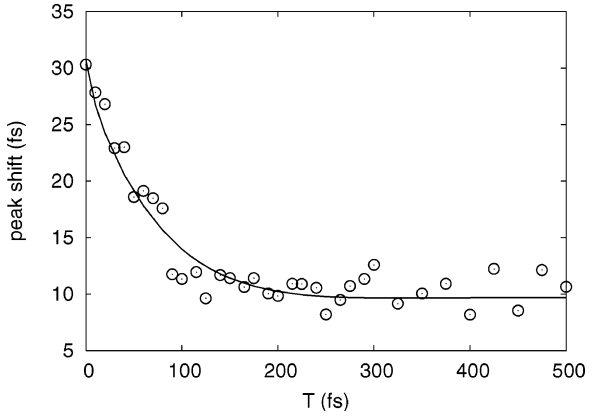

Figure 2. Comparison of numerical methods for the average over static disorder. We show the peak shift results calculated using the 11-point Gauss−Hermite method (solid line) and Monte Carlo sampling using 5000 points (open circles). The model system is a two-level system (ground state and a singlely excited state) with bath parameters: $\lambda_0 = 150\ \mathrm{cm}^{-1}$, $\Omega_0 = 50\ \mathrm{cm}^{-1}$, $\Gamma_0 = 80\ \mathrm{cm}^{-1}$, and Gaussian static energy disorder with $\sigma_s = 100\ \mathrm{cm}^{-1}$. The pulse width used in the simulations is 20 fs.

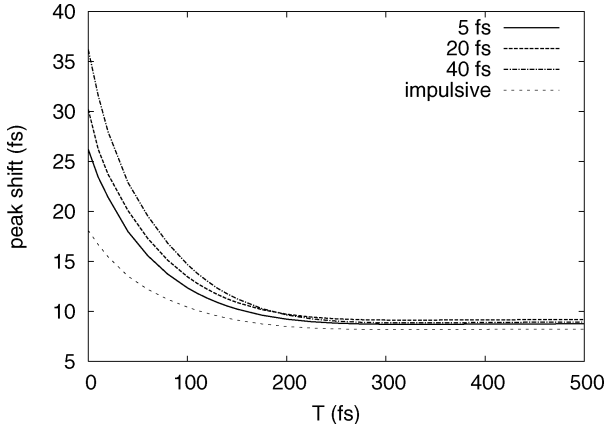

Figure 3. Pulse-overlap effects in simulated 3PEPS signals. The model system is a two-level system (ground state and a single excited state) with bath parameters: $\lambda_0 = 150\ \mathrm{cm}^{-1}$, $\Omega_0 = 50\ \mathrm{cm}^{-1}$, $\Gamma_0 = 80\ \mathrm{cm}^{-1}$, and Gaussian static energy disorder with $\sigma_s = 100\ \mathrm{cm}^{-1}$.

by using the response function approach in the impulsive limit is also shown.[1] Clearly, a significant portion of the initial peak shift decay at $T < 100$ fs is due to the pulse overlap effect. In addition, a longer pulse duration results in larger initial peak shift, as expected.[9]

4. 1C- and 2C3PEPS of a Bacterial RC: Electronic Coupling between H and B

In this section, we turn our attention to a specific experiment and demonstrate that the theoretical method presented in Section 2 can be applied to simulate 3PEPS decay in a bacterial photosynthetic reaction center (RC) and determine the electronic coupling constant between the bacteriopheophytin and accessory bateriochlorophyll in the RC.

We focus on one-color (1C) and two-color (2C) 3PEPS data for the RC of the photosynthetic purple bacterium *Rhodobacter sphaeroides*, whose primary electron donor P is chemically oxidized. The RC contains two bateriochorophylls constituting the special pair (P), an accessory bateriochorophyl adjacent to P on each side (BChl; B_A and B_B), and a bateriopheophytin next to each B (BPhy; H_A and H_B).[42,43] The RC converts harvested solar energy into chemical charge separation with a quantum yield near 1 in about 3 ps at room temperature.[44−47] In addition, in the isolated RC, energy transfer occurs from H to B in about 100 fs and from B to P in about 150 fs.[48−52] Oxidation of the special pair of the RC by $K_3Fe(CN)_6$ in our experiment blocks electron transfer from P to H_A, however, the downward energy transfer from H to B to P still occurs in a time scale similar to the neutral RC.[51−53] Knowing the coupling constant between B and H is critical for the understanding of the rapid energy transfer from H to B, and the 2C3PEPS technique provides an experimental probe for the electronic coupling. However, given that the energy transfer from H to B occurs in ∼100 fs time scale and the pulse duration in the experiment is ∼40 fs, it is clear that both the energy transfer dynamics and pulse-overlap effects must be treated properly to account for the peak shift decay in the 100 fs time scale.

The 3PEPS technique has been used to study the electron−phonon couplings in a neutral RC at room temperature and 77 K.[15,20] In ref 20, the 1C- and 2C3PEPS experiments were performed and used to estimate the electronic coupling between H and B in the neutral RC. In that work, Parkinson et al. used response function formalism to describe 3PEPS. By fitting to the 1C3PEPS, they obtained line shape function of individual chromophores. Assuming the fluctuations of transition energies on H and B are independent, they were able to estimate an H−B coupling constant of $\sim 170\ \mathrm{cm}^{-1}$ by fitting to the uphill 2C3PEPS data. However, the downhill 2C3PEPS data was not well described by the response function formalism, presumably because the rapid energy transfer and direct charge separation dynamics in the RC is not properly described by the response functions. Here, we will adopt a similar scheme to estimate the electronic coupling between H and B in the P-oxidized RC and demonstrate that the present theoretical method can adequately describe all four 3PEPS experiments.

4.1. Methods and Materials. His-tagged *Rhodobacter sphaeroides* cells were kindly supplied by the Boxer lab. They were grown and the RC was purified as published previously.[51] Briefly, cells were grown in semi-aerobic and dark conditions. By using a French press, we disrupted the cells and solubilized the RC with the detergent laurydimethylamide oxide (LDAO). Purification was carried out with a Ni-NTA column, followed by a DEAE column. After concentration of the sample, ∼100 mM of $K_3Fe(CN)_6$ was added to oxidize the primary electron donor, P, just prior to the experiment. The samples were diluted with 60% v/v glycerol and placed in a 0.2 mm quartz cell (Starna) for measurements. The optical density of the sample at 800 nm was 0.1−0.3. Figure 4 shows the absorption spectrum of the P-oxidized RC at 77 K, showing the H band at 750 nm and the B band at 800 nm. The oxidation of the special pair was confirmed by both the absorption spectrum (Figure 4) and a 800 nm one-color transient absorption (TA) measurement; both the P band in the absorption spectrum and the several picosecond rising components in the 800 nm TA signal due to charge separation disappear.[51] The 800 nm one-color TA experiments were also carried out before and after each scan to confirm the integrity of the sample, and our data were consistent with the literature.[51] The experiments were performed at 77 K using an Optistat DN cryostat from Oxford Instruments.

Our setup for the 3PEPS experiments was described in detail elsewhere,[9,16,54] and here we briefly describe relevant details for the completeness of this work. The 800 and 750 nm laser pulses were chosen to be on resonance with the B and H transitions, respectively (Figure 4). The 800 nm pulse was generated from a home-built regenerative amplifier at 1 kHz, which was seeded by a Femtosource Compact Pro Ti:sapphire oscillator (Femtolasers, Inc.) Part of this beam was used to pump

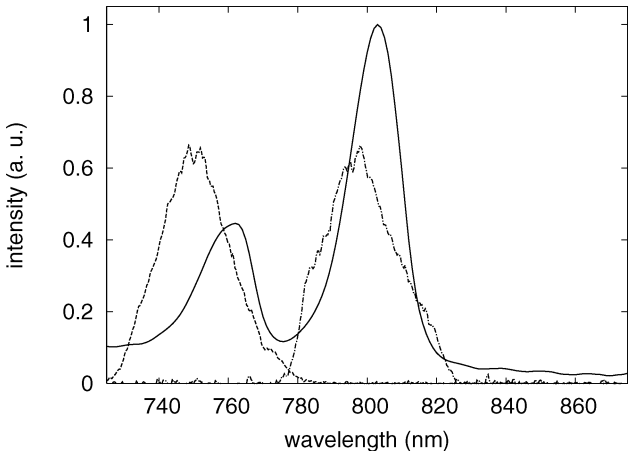

Figure 4. Linear absorption spectrum of the P-oxidized RC at 77 K (solid line). The spectrum consists of two absorption bands labeled as H and B, which correspond to the excitations mainly on the accessory bacteriochlorophyll and the bacteriopheophytin molecules, respectively. The spectral profiles of the 750 nm (dashed line) and 800 nm (dash−dotted line) pulses are also shown. The 750 nm pulse is on resonance with the H band, and the 800 nm pulse is on resonance with the B band.

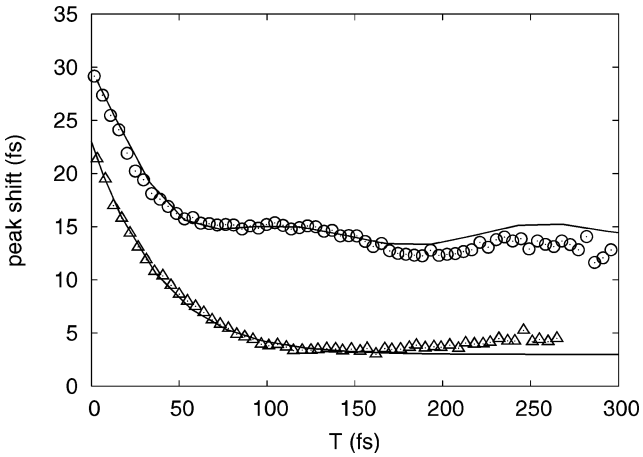

Figure 5. One-color three-pulse photon-echo peak shift for the P-oxidized RC. The 1C3PEPS results using pulses centered at 750 nm (H band, open triangle) and at 800 nm (B band, open circle) measured at 77 K are shown. The solid lines are simulations using bath parameters listed in Table 1.

an optical parametric amplifier (Coherent 9450) to produce a 750 nm pulse. This was passed through an optical filter centered at 750 nm with bandwidth of 25 nm. Both pulses were measured to have ∼40 fs fwhm pulse duration at the sample position. Figure 4 shows the spectral profiles of the laser pulses; note that the spectral overlap between the pulses is minimal, that each pulse overlaps with most of the corresponding spectral band, and that each pulse has negligible overlap with the other spectral band. In the experiments, the total input power was kept between 1 and 5 μW.

The three pulses were arranged in equilateral triangle geometry and focused onto the sample with a 20 cm singlet lens. Four 3PEPS experiments were carried out on the RC. For the one-color experiments, three pulses of the same wavelength (750 nm or 800 nm in this case) were used. For two-color experiments, the first two pulses were set to a pump wavelength, while the third pulse was set to a probe wavelength. Two different types of 2C3PEPS scans were carried out in this work. In the first, the "downhill" experiment, the pump wavelength is set to 750 nm and the probe wavelength is set to 800 nm. In the second, the "uphill" experiment, the pump wavelength is set to 800 nm and the probe wavelength is set to 750 nm. Integrated echo profiles were measured as a function of the coherence time τ for fixed values of the population time T. The peak shift for a given population time is the value of the coherence time that gives the maximum signal as determined by fitting to a single Gaussian function. The integrated photon-echo signal is collected on a photomultiplier tube (PMT) in the phase-matching direction. For the two-color experiments, 25 nm bandwidth filters corresponding to the probe wavelengths were placed in front of the PMT to prevent scattering from the pump beams. Data were collected using an optical chopper and lock-in amplifier.

4.2. Theoretical Model for the RC. To simulate the peak shift, we consider a coupled heterodimer system representing the coupled accessory BChl and BPhy molecules on the same branch. The transition dipole moments for the Q_y transitions on the accessory BChl and BPhy are taken from the semiempirical quantum chemistry study in ref 52. In general, peak shift decay is relatively insensitive to the transition dipole of excitations,[19] therefore we fix the transition dipole moments and do not treat them as fitting parameters. In addition, we assume the bath modes coupled to the accessory BChl and BPhy are independent and the electronic couplings are small compared to the site energy difference between them so that the main characters of the H band and B band are the localized BPhy and accessory BChl Q_y excitations, respectively. In this limit, we can use the 1C3PEPS data at 750 and 800 nm to directly determine the spectral density of bath modes coupled to BPhy and accessory BChl.

For the system−bath interactions, we consider diagonal system−bath couplings in the site representation that modulate the site energies of BChl and BPhy Q_y excitations and treat the bath parameters in the spectral density (eq 17) as free parameters to be determined by fitting to the 1C3PEPS experiments. Note that, in the present model, the H → B energy transfer dynamics is determined by the system Hamiltonian and the bath parameters according to the TNL quantum master equation in eq 20. To include the rapid B → P^+ population transfer in our simulations, we consider an additional P^+ state acting as an energy sink that traps population from B. This additional population transfer channel is included by adding a dark state in the Hamiltonian and an additional Markovian Lindblad population transfer term[34] with time constant of 150 fs in the quantum master equation (eq 20). In our 2C3PEPS simulations, we found that this term is necessary to reproduce the negative 2C3PEPS observed in the experiments.

4.3. Results and Discussion. Figures 5 and 6 show the 1C3PEPS and 2C3PEPS of the P-oxidized RC. The 1C3PEPS measurements on B and H both show very rapid peak shift decay in about 100 fs, and then a plateau between 100 to 200 fs. In addition, quite different initial peak shifts and residual peak shifts at $T \sim 300$ fs are observed, indicating that the excitation−phonon couplings for B and H are different. Note that we only show the peak shift for population times up to $T = 300$ fs because the intensity of the 3PPE signal at $T > 300$ fs is small and the signal is noisy. This is because the vary rapid H to B to P^+ energy transfer removes the population and causes the 3PPE signal to decay rapidly. Thus, we will focus our analysis on the data between $T = 0$ and $T = 300$ fs. Clearly, the peak shift does not decay to zero in this time scale, which means some nuclear motion is static in this time scale. A noticeable feature in the 2C3PEPS data is the negative peak shift, which is also observed in the neutral RC and was considered to be the effect due to the rapid population dynamics.[20]

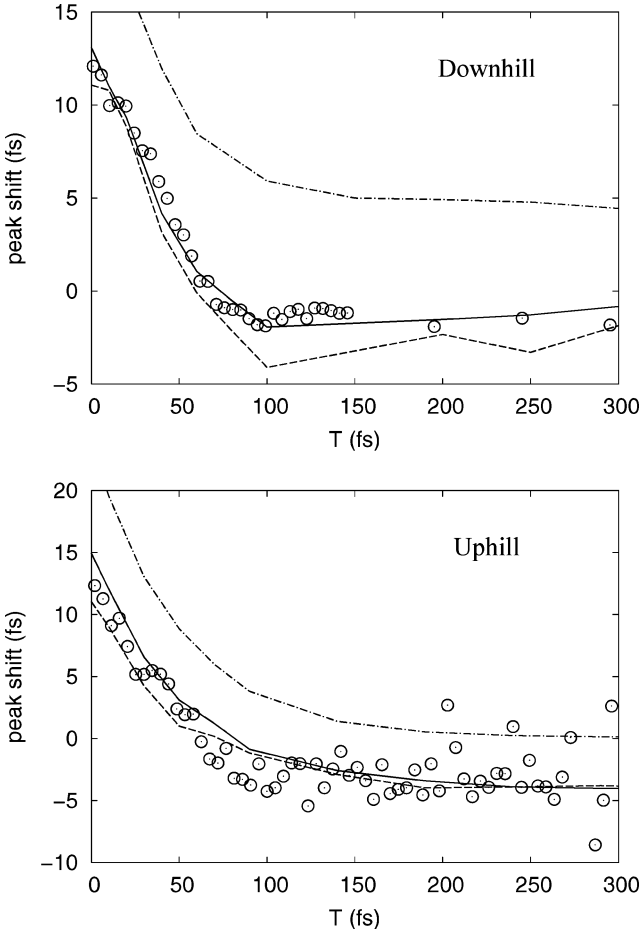

Figure 6. Two-color three-pulse photon-echo peak shift for the P-oxidized RC (open circle). The 2C3PEPS results at 77 K using downhill (upper panel) and uphill (lower panel) pulse sequences are shown. The solid lines are simulations using the bath parameters listed in Table 1 and an electronic coupling constant $J = 250$ cm^{-1}. Simulations using different couplings $J = 200$ and 300 cm^{-1} are shown as dashed and dash−dotted lines, respectively.

TABLE 1: Bath Parameters for H and B of the P-oxidized RC of *Rb. sphaeroides* Obtained from 1C3PEPS Measurements (cm^{-1})

		λ^a	Ω^a	Γ^a	σ^b
accessory	BChl	75	100	150	60
		1500	220	10	
	BPhy	250	50	150	60

[a] Coupling strength λ, characteristic frequency Ω, and damping constant Γ defined in eq 17. [b] Standard deviation of the Gaussian static disorder.

In Figure 5, we show the 1C3PEPS simulations calculated using the theoretical method described in Section 2. The bath parameters used to reproduce the experiments are listed in Table 1. We found that the B band 1C3PEPS data requires two bath terms to describe it adequately, while the H band 1C3PEPS data can be reasonably reproduced by a single overdamped oscillator term. This is mainly due to the structure around $T =$ 150 fs on the B band 1C3PEPS. Note that the 220 cm^{-1} mode is also observed in the 1C3PEPS and Raman measurements for the neutral RC at room temperature, in agreement with our result.[15,55] Our numerical simulation indicates that the plateau observed in the B band 1C3PEPS at $T \sim 150$ fs is due to the interference between vibrational contributions. Note that the simulations reproduce the peak shifts measured at small T, indicating the improvement due to the proper inclusion of pulse-overlap effects. This is critical for the current study. Because the peak shift decays on the 100 fs time scale and reliable data is only available for $T < 300$ fs, to obtain a meaningful interpretation of the experimental data, one needs to be able to describe the sub-100 fs part of the peak shift decay. Moreover, the inhomogeneous Gaussian static disorder with $\sigma = 60$ cm^{-1} obtained from 1C3PEPS experiment on the accessory pigments of the RC is in good agreement with the value reported previously in the room-temperature 1C3PEPS and Raman studies.[15,55]

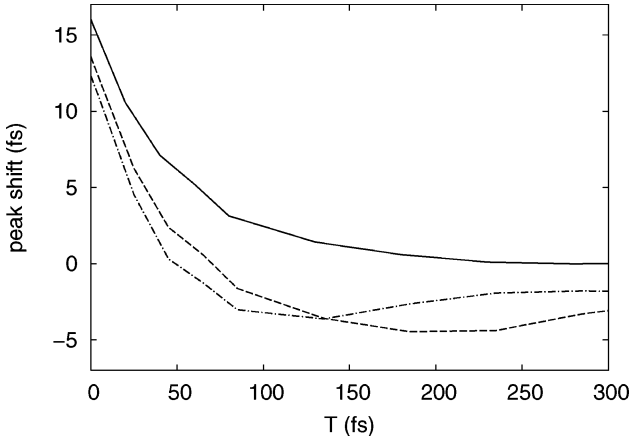

Figure 7. Effects of rapid energy transfer on the uphill 2C3PEPS. We show simulated curves of the uphill 2C3PEPS without B → P$^+$ population transfer (solid line) and with B → P$^+$ population transfer at 100 fs (dashed line) and 50 fs (dash−dotted line). The additional population transfer channels were included by adding additional Lindblad terms in the quantum master equation. In the simulations, the bath parameters listed in Table 1 and $J = 250$ cm^{-1} were used.

We use the bath parameters extracted from the 1C3PEPS data (Table 1) to simulate the 2C downhill and uphill experiments. By varying the electronic coupling constant J with the constraint that the energy difference between the excitonic H and B states is fixed at 680 cm^{-1}, we found a value of $J = 250$ cm^{-1} gives the best fit to both measurements. The simulated 2C downhill and uphill 3PEPS are shown in Figure 6, in which simulations with $J = 200$ cm^{-1} and 300 cm^{-1} are also shown to demonstrate that the 2C3PEPS measurement is sensitive to the electronic couplings. The estimated value of $J = 250$ cm^{-1} is slightly larger than the value observed in the wild-type RC[20] ($J = 170$ cm^{-1}) and the theoretical value calculated using semiemprical quantum chemistry method[52] ($J = 200$ cm^{-1}); the larger J may explain the rapid H to B excitation energy transfer.

The negative peak shifts observed in the 2C3PEPS experiment were attributed by Parkinson et al. to the rapid energy transfer dynamics in the RC.[20] For example, in the 2C uphill experiment, the B → P$^+$ energy transfer rapidly removes population on B during the time period between the second and the third pulses and significantly reduces the total signal strength as the time increases. The negative peak shift occurs because, at a given population time T, the time period between the second and the third pulses decreases when the coherence time τ becomes more negative (Figure 1). Our dynamical simulations confirmed this explanation and showed that the rapid B → P$^+$ energy transfer is responsible for the negative peak shifts in both the uphill and downhill experiments. In Figure 7, we compare theoretical uphill 2CPEPS simulations with B → P$^+$ population transfer to simulations without B → P$^+$ population transfer. Clearly, the population dynamics in general reduces the peak shift and gives rise to negative peak shifts at short T. The effects in the downhill 2C3PEPS are an interplay of the B → P$^+$ dynamics, which

reduces signal strength and causes negative peak shifts, and the H → B dynamics, which actually generates additional signals. As a result, the downhill 2C3PEPS is less negative compared to the uphill 2C3PEPS and is almost flat after the bath relaxation time scale (Figure 6).

Note that we assume that the bath mode coupled to chromophores H and B are uncorrelated, which should be a good approximation for chromophores that are spatially far apart. However, in a densely packed protein−pigment complex such as the RC, in which the center-to-center distance between BPhy and BChl chromophores is about 10 Å, the uncorrelated bath assumption is likely to be broken. A recent experiment in our group shows that the transition energy fluctuations on BPhy and BChl are highly correlated, which results in a long-lasting coherence between H and B excitonic states and indicates that a theoretical model that includes correlated bath dynamics and coherent energy transfer dynamics is needed to describe the system.[56] In this case, the present theoretical method for third-order nonlinear spectroscopy can be extended to include nonlocal bath effects by considering system−bath coupling terms with nonlocal system operators. Work is currently in progress to extend the present approach to include nonlocal bath effects and refine our estimate of the electronic coupling.

5. Conclusions

We have combined a time-nonlocal non-Markovian quantum master equation[37] and a perturbative scheme[30] for the calculation of the third-order polarization in the phase-matching direction $\mathbf{k_s} = -\mathbf{k_1} + \mathbf{k_2} + \mathbf{k_3}$ to calculate the three-pulse photon-echo signals. We have extended the formalism proposed by Gelin et al. to describe multichromophoric systems with a two-excitation manifold, thus enabling the calculation of general three-pulse photon-echo signals. In addition, an efficient numerical integration scheme based on the Gauss−Hermite quadrature rule was used to perform an average over a statistical Gaussian distribution of transition frequencies and thus include the effects of static disorder. This allows the efficient calculation of three-pulse photon-echo peak shifts of coupled chromophores in condensed phase environments.

Compared to the standard perturbative approach of nonlinear spectroscopy, this new scheme has several key advantages. First, unlike the standard approach that works in the impulsive limit and RWA, the present method incorporates all relevant optical fields into the system Hamiltonian and propagates the driven dynamics of the system numerically. Therefore, arbitrary pulse durations can be used in the simulations and all pulse-overlap effects are automatically accounted for. This enables us to correctly simulate 3PEPS at short population times. Second, because we use a time-nonlocal non-Markovian theory, all relevant dissipative dynamics of the system are included in the new method. For example, effects of coherent energy transfer and non-Markovian dynamics are included in a unified manner, which would be difficult to implement in the standard perturbative approach. Third, no additional effort is needed to apply this method to systems with a time-dependent Hamiltonian. This should be useful for study of a system whose electronic Hamiltonian is modulated by slow nuclear coordinates.

We applied the theoretical method to simulate one-color and two-color 3PEPS experiments on a bacterial reaction center whose special pair is chemically oxidized. With the new theoretical approach, we are able to reproduce all experimental results simultaneously and determine that the electronic coupling $J = 250\ \mathrm{cm}^{-1}$ between the localized Q_y excitations on the bacteriopheophytin and accessory bateriochlorophyll in the RC.

Recently, two-dimensional (2D) electronic spectroscopy has been shown to be an effective probe of electronic couplings and dynamical information in multichromophoric systems.[3,57−60] The 2D technique is complementary to the 3PEPS measurements described in this work.[19] Because the 2D spectra can be calculated by performing a double Fourier transform on $P^{(3)}_{3\mathrm{PPE}}(\tau,T,t)$, the theoretical method presented in this work can be used to calculate 2D spectra without any modification. Because the full dynamics and pulse-overlap effects are incorporated, the current method will also be useful for the interpretation of 2D electronic spectroscopic measurements.

Acknowledgment. This work was supported by the Office of Basic Energy Sciences, Chemical Sciences Division, U.S. Department of Energy (contract DE-AC03-76SF000098). We would like to thank S. Boxer for *Rhodobacter sphaeroides* samples and B. S. Prall and D. Y. Parkinson for valuable discussions. We thank E. A. Berry, L. S. Huang, and N. G. Pon for generous help with sample preparation.

References and Notes

(1) Mukamel, S. *Principles of Nonlinear Optical Spectroscopy*; Oxford University Press: Oxford, 1995.
(2) Mukamel, S. *Annu. Rev. Phys. Chem.* **2000**, *51*, 691.
(3) Jonas, D. M. *Annu. Rev. Phys. Chem.* **2003**, *54*, 425.
(4) Jimenez, R.; van Mourik, F.; Yu, J. Y.; Fleming, G. R. *J. Phys. Chem. B* **1997**, *101*, 7350.
(5) Nagasawa, Y.; Yu, J. Y.; Cho, M. H.; Fleming, G. R. *Faraday Discuss.* **1997**, *108*, 23.
(6) Agarwal, R.; Krueger, B. P.; Scholes, G. D.; Yang, M.; Yom, J.; Mets, L.; Fleming, G. R. *J. Phys. Chem. B* **2000**, *104*, 2908.
(7) Ohta, K.; Yang, M.; Fleming, G. R. *J. Chem. Phys.* **2001**, *115*, 7609.
(8) Vaswani, H. M.; Stenger, J.; Fromme, P.; Fleming, G. R. *J. Phys. Chem. B* **2006**, *110*, 26303.
(9) Joo, T.; Jia, Y.; Yu, J.; Lang, M.; Fleming, G. R. *J. Chem. Phys.* **1996**, *104*, 6089.
(10) Cho, M.; Yu, J.; Joo, T.; Nagasawa, Y.; Passino, S.; Fleming, G. R. *J. Phys. Chem.* **1996**, *100*, 11944.
(11) Passino, S. A.; Nagasawa, Y.; Fleming, G. R. *J. Chem. Phys.* **1997**, *107*, 6094.
(12) Nagasawa, Y.; Passino, S. A.; Joo, T.; Fleming, G. R. *J. Chem. Phys.* **1997**, *106*, 4840.
(13) Nagasawa, Y.; Yu, J. Y.; Fleming, G. R. *J. Chem. Phys.* **1998**, *109*, 6175.
(14) Yu, J. Y.; Nagasawa, Y.; van Grondelle, R.; Fleming, G. R. *Chem. Phys. Lett.* **1997**, *280*, 404.
(15) Groot, M. L.; Yu, J.; Agarwal, R.; Norris, J.; Fleming, G. R. *J. Phys. Chem. B* **1998**, *102*, 5923.
(16) Prall, B. S.; Parkinson, D. Y.; Fleming, G. R. *J. Chem. Phys.* **2005**, *123*, 054515.
(17) Yang, M.; Fleming, G. R. *J. Chem. Phys.* **1999**, *111*, 27.
(18) Mancal, T.; Fleming, G. R. *J. Chem. Phys.* **2004**, *121*, 10556.
(19) Cho, M.; Fleming, G. R. *J. Chem. Phys.* **2006**, *123*, 114506.
(20) Parkinson, D. Y.; Lee, H.; Fleming, G. R. *J. Phys. Chem. B* **2007**, *111*, 7449.
(21) Meier, T.; Chernyak, V.; Mukamel, S. *J. Chem. Phys.* **1997**, *107*, 8759.
(22) Zhang, W. M.; Meier, T.; Chernyak, V.; Mukamel, S. *J. Chem. Phys.* **1998**, *108*, 7763.
(23) Yang, M.; Fleming, G. R. *J. Chem. Phys.* **2000**, *113*, 2823.
(24) Seidner, L.; Stock, G.; Domcke, W. *J. Chem. Phys.* **1995**, *103*, 3998.
(25) Wolfseder, B.; Seidner, L.; Stock, G.; Domcke, W. *Chem. Phys.* **1997**, *217*, 275.
(26) Kato, T.; Tanimura, Y. *Chem. Phys. Lett.* **2001**, *341*, 329.
(27) Kjellberg, P.; Pullerits, T. *J. Chem. Phys.* **2006**, *124*, 024106.
(28) Mancal, T.; Pisliakov, A. V.; Fleming, G. R. *J. Chem. Phys.* **2006**, *124*, 234504.
(29) Pisliakov, A. V.; Mancal, T.; Fleming, G. R. *J. Chem. Phys.* **2006**, *124*, 234505.
(30) Gelin, M. F.; Egorova, D.; Domcke, W. *J. Chem. Phys.* **2005**, *123*, 164112.
(31) Renger, T.; May, V.; Kuhn, O. *Phys. Rep.* **2001**, *343*, 137.
(32) Bakalis, L. D.; Knoester, J. *J. Chem. Phys.* **1997**, *106*, 6964.
(33) Redfield, A. G. *IBM J. Res. Dev.* **1957**, *1*, 19.

(34) Breuer, H.-P.; Petruccione, F. *The Theory of Open Quantum Systems*; Oxford University Press: Oxford, 2002.
(35) Weiss, U. *Quantum Dissipative Systems*; World Scientific: Singapore, 2001.
(36) Kleinekathafer, U. *J. Chem. Phys.* **2004**, *121*, 2505.
(37) Meier, C.; Tannor, D. J. *J. Chem. Phys.* **1999**, *111*, 3365.
(38) Press, W. H.; Flannery, B. P.; Teukolsky, S. A.; Vetterling, W. T. *Numerical Recipes in C: The Art of Scientific Computing*; Cambridge University Press: New York, 1992.
(39) Durrant, J. R.; Knoester, J.; Wiersma, D. A. *Chem. Phys. Lett.* **1994**, *222*, 450.
(40) Abramowitz, M.; Stegun, I. A. *Handbook of Mathematical Functions with Formulas, Graphs, and Mathematical Tables*, 9th Dover printing, 10th GPO printing ed.; Dover: New York, 1964.
(41) Lu, J.; Darmofal, D. L. *SIAM J. Sci. Comput.* **2004**, *26*, 613−624.
(42) Chang, C. H.; el Kabbani, O.; Tiede, D.; Norris, J.; Schiffer, M. *Biochemistry* **1991**, *30*, 5352.
(43) Ermler, U.; Fritzsch, G.; Buchanan, S. K.; Michel, H. *Structure* **1994**, *2*, 925.
(44) Woodbury, N. W.; Becker, M.; Middendorf, D.; Parson, W. W. *Biochemistry* **1985**, *24*, 7516.
(45) Martin, J. L.; Breton, J.; Hoff, A. J.; Migus, A.; Antonetti, A. *Proc. Natl. Acad. Sci. U.S.A.* **1986**, *83*, 957.
(46) Fleming, G. R.; Martin, J. L.; Breton, J. *Nature* **1988**, *333*, 190.
(47) Lin, S. H.; Chang, C. H.; Liang, K. K.; Chang, R.; Shiu, Y. J.; Zhang, J. M.; Yang, T.-S.; Hayashi, M.; Hsu, F. C. *Adv. Chem. Phys.* **2002**, *121*, 1.
(48) Stanley, R. J.; King, B.; Boxer, S. G. *J. Phys. Chem.* **1996**, *100*, 12052.
(49) Jonas, D. M.; Lang, M. J.; Nagasawa, Y.; Joo, T.; Fleming, G. R. *J. Phys. Chem.* **1996**, *100*, 12660.
(50) Vos, M. H.; Breton, J.; Martin, J. L. *J. Phys. Chem. B* **1997**, *101*, 9820.
(51) Jackson, J.; Lin, S.; Taguchi, A. K.; Williams, J.; Allen, J.; Woodbury, N. *J. Phys. Chem. B* **1997**, *101*, 5747.
(52) Jordanides, X.; Scholes, G. D.; Shapley, W.; Reimers, J.; Fleming, G. R. *J. Phys. Chem. B* **2004**, *108*, 1753.
(53) Jonas, D. M.; Lang, M. J.; Nagasawa, Y.; Bradforth, S. E.; Dikshit, S. N.; Jimenez, R.; Joo, T.; Fleming, G. R. Ultrafast Energy Transfer within the Bacterial Photosynthetic RC. *Proceedings of the Feldafing III Workshop*, Munich, 1995.
(54) Agarwal, R.; Prall, B. S.; Rizvi, A.; Yang, M.; Fleming, G. R. *J. Chem. Phys.* **2002**, *116*, 6243.
(55) Cherepy, N.; Shreve, A.; Moore, L.; Boxer, S. G.; Mathies, R. *J. Phys. Chem. B* **1997**, *101*, 3250.
(56) Lee, H.; Cheng, Y.-C.; Fleming, G. R. *Science* **2007**, *316*, 1462.
(57) Brixner, T.; Mancal, T.; Stiopkin, I. V.; Fleming, G. R. *J. Chem. Phys.* **2004**, *121*, 4221.
(58) Brixner, T.; Stenger, J.; Vaswani, H. M.; Cho, M.; Blankenship, R. E.; Fleming, G. R. *Nature* **2005**, *434*, 625.
(59) Nagy, A.; Prokhorenko, V.; Miller, R. J. *Curr. Opin. Struct. Biol.* **2006**, *16*, 654.
(60) Engel, G. S.; Calhoun, T. R.; Read, E. L.; Ahn, T. K.; Mancal, T.; Cheng, Y.-C.; Blankenship, R. E.; Fleming, G. R. *Nature* **2007**, *446*, 782.